inter·noise 2023
CHIBA,GREATER TOKYO 20-23 AUGUST

Development of a UAV Test Stand

Jared Schmal [1]
D. W. Herrin [2]
University of Kentucky
151 Ralph G. Anderson Building
Lexington, KY 40506-0503
USA

Daniel Fernández Comesaña[3]
Microflown Technologies
Tivolilaan 205
6824 BV Arnhem
The Netherlands

ABSTRACT

Performing acoustic measurements on a multicopter in a confined space, such as a small anechoic chamber, can be an extremely difficult and time-consuming process. Inherent risks to the vehicle, laboratory equipment, and technicians are present when a multicopter is operated. In addition, standard multicopter maneuvers are difficult to conduct due to spatial constraints, and obtaining near field acoustic measurements is dangerous due to the inherent dynamic variability that occurs during flight. A UAV test stand was developed to remove these limitations and allow for rapid and safe acoustic measurements in a controlled environment. The design, development, and initial measurements are discussed. The performance and acoustic response of the brushless electric motors and propellers are assessed to examine the effectiveness of the test stand. The contribution noise from the test stand and a measurement grid are evaluated, as well as the influence of stationary propeller testing. Lastly, the pros and cons of using a test stand for UAV measurements are discussed.

1. INTRODUCTION

The rapid development of Unmanned Aerial Vehicles (UAVs) over the past ten years has generated a booming market in the recreational, commercial, and military sectors. These vehicles have been designed for a myriad of applications, such as photography and film, surveying and mapping, infrastructure inspections, package delivery, search and rescue, and agricultural spraying. The adoption and utilization of UAVs continue to grow as new and innovative uses are discovered. Vibro-acoustics has been a research and development focus, and this is expected to continue well into the future as noise pollution is a major hurdle for public acceptance of UAVs.

The acoustic behavior of UAVs is not fully understood. Many sources contribute to the overall sound, and the generated acoustic field is complex. Understanding the physical source mechanisms is a critical first step for evaluating prediction models and designing modifications for quieter operations. However, difficulties arise in UAV measurements due to the complexity of replicating

[1] Email: jared.schmal@uky.edu
[2] Email: david.herrin@uky.edu
[3] Email: fernandez@microflown.com

standard maneuvers in a controlled environment. Inherent risks to the vehicle, laboratory equipment, and technicians are present when a UAV is operated in an anechoic chamber. In addition, many standard acoustic measurements, such as sound intensity scans in the near field, are difficult to conduct due to the dynamic variability that occurs during flight. The development of a UAV test stand would remove these limitations to allow for rapid and safe measurements in a controlled environment.

The majority of academic research to date has focused on test stands that examine a single component and use microphones to measure sound pressure in the far field. In this paper, sound pressure and particle velocity measurements in the near and far field were completed using a UAV test stand in a quadcopter configuration. A thorough analysis was conducted to determine the effectiveness of the UAV test stand as well as the contribution noise from the stand, measurement equipment, and testing environment.

2. BACKGROUND

A quadcopter can be broken down into three major subsystems: a) airframe, b) propulsion, and c) command and control. The airframe consists of the fuselage, arms, and landing gear. Propellers, motors, electronic speed controllers (ESCs), and batteries are grouped in the propulsion category. The command and control system includes the flight controller, transmitter and receiver, ground control station, and relevant sensors [1]. The selection of each of these systems is highly customizable and dependent on the vehicle design parameters. While each of these categories is equally important to the vehicle operation, the acoustic contribution is limited to several components. The primary acoustic source of a quadcopter is contained in the propulsion system, although the airframe noise contribution can also be significant depending on the design. The command and control system does not contribute to the noise, although advancements in flight controller software or routing can reduce the noise impact on the receivers.

The propellers are responsible for generating the thrust required to counter the force of gravity and are the primary acoustic source of a quadcopter in most cases [2]. The tonal response of a propeller occurs at the blade pass frequency (BPF) and its harmonics. The BPF is defined as

$$f_{\mathrm{BP}n} = \frac{nNR}{60} \ [Hz] , \tag{1}$$

where n is an integer, N is the number of blades, and R is the revolutions per minute of the motor shaft [3]. Several variables that impact propeller noise are the material, pitch, and number of blades [4], but the most significant acoustic factor is reducing the blade tip speed [5].

The airframe can also be an important acoustic source due to interaction noise between the propeller and quadcopter arm [6]. The tip clearance (Δ) is defined as the distance between the propeller tip and the airframe arm. Zawodny and Boyd found amplifications in tonal amplitude when the tip clearance is adjusted, resulting in a significant increase in the overall sound pressure level (OASPL) at positions outside the propeller plane [7]. A negligible influence was discovered by maintaining a ratio of

$$\frac{\Delta}{r} \geq 0.5 , \tag{2}$$

where Δ is the tip clearance and r is the radius of the propeller. The armature geometry, if constant, has been shown to have little impact on the acoustic response [8]. Zawodny and Boyd discovered the armature width is more critical [7]. A substantial decrease in airframe noise can be achieve by maintaining a ratio of

$$\frac{W}{c_{0.75r}} \leq 1.08\,, \tag{3}$$

where W is the cross sectional length of the airframe and $c_{0.75r}$ is the cross sectional length of the propeller at 75% of the tip radius [7].

3. UAV STAND DESIGN

The primary design parameters of the UAV test stand included ease of customization to allow for testing of different multicopter configurations and components, the ability to emulate flight maneuvers and monitor hardware performance, and to limit the stand interference. The final setup can be seen in Figure 1.

Figure 1: Final design of the UAV test stand.

3.1. Airframe

The airframe of the UAV test stand was constructed using 80/20 aluminum T-slot framing. Rubber feet are used to isolate the stand from the floor. Motor mounts and a top plate were designed to enable testing of different airframe configurations. Each arm can be rotated from 0 – 90 degrees and the motor mounts can slide along the length of the arm to allow for testing of various multicopter sizes. A minimum wheelbase (diagonal length between each motor rotor) of 18 cm and a maximum wheelbase of 112 cm can be tested using the current setup.

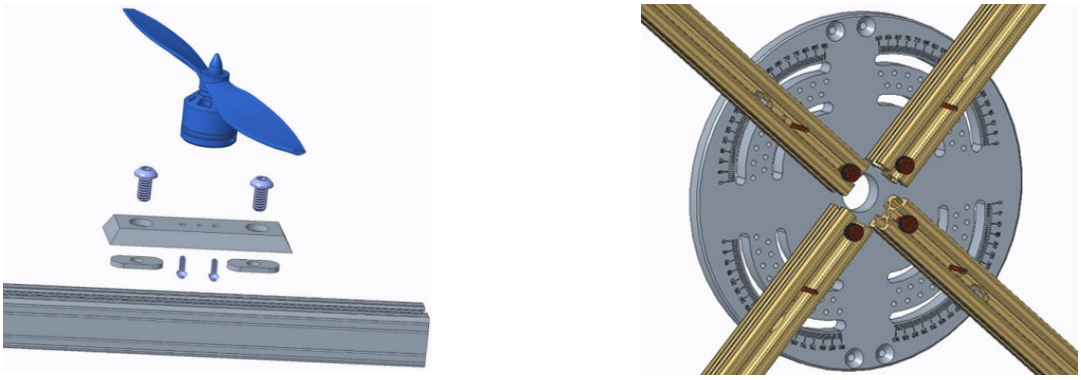

Figure 2. UAV test stand motor mounts (left) and top plate with adjustable arms (right).

The stand was designed in a vertical configuration, with the flow propagating parallel to the floor, to ease measurement scanning in the near field and along propagation planes. This configuration is also thought to reduce reflections and flow interference when testing in a hemi-anechoic chamber.

3.2. Propulsion

The test stand is currently configured to replicate a Foxtech Hover 1 quadcopter, a customizable multicopter currently being used for control research at the University of Kentucky. XRotor 40A ESCs are used with T-Motor MN3508 brushless electric direct current (BLDC) motors with a KV-rating of 380. The KV-rating defines the rotational rate of the motor without a load for each volt applied [1]. Foldable carbon composite propellers have been installed with high strength aluminum alloy motor mounts. The length of each propeller is 38.1 cm with a 13.2 cm pitch. The test stand is powered by two DC power supplies that can simulate a six-cell battery pack with a nominal voltage of 22.2 V.

3.3. Command and Control

A RC transmitter or ground control station is typically used to command a UAV, while an autopilot combined with a variety of sensors is used for control. A simplified system could be used for the test stand since the objective is to control and monitor the rotation rate of each propeller. A computer is used to send commands to an Arduino Mega 2560 micro controller that allows each motor to be controlled and monitored independently. The Arduino sends pulse width modulation (PWM) signals to the ESCs as well as powers and records sensor information. The current input and the RPM of each propeller was individually monitored using hall effect and infrared (IR) sensor modules. A wiring diagram can be seen in Figure 3.

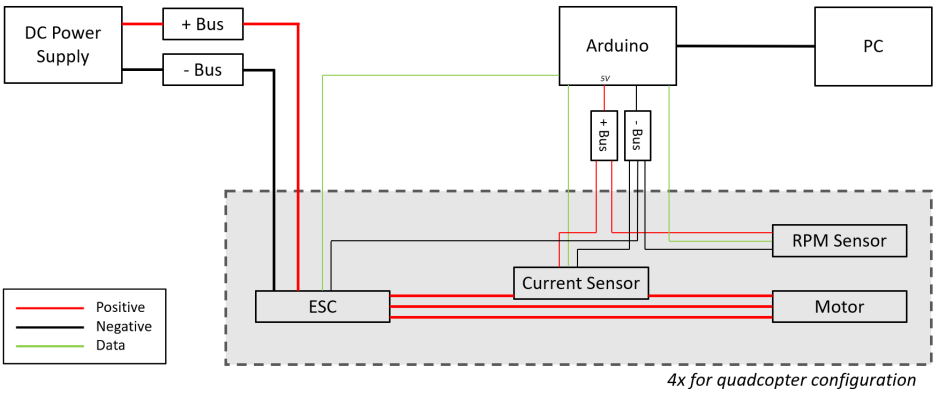

Figure 3. Wiring diagram for the command and control system of the UAV test stand.

The test stand is capable of replicating the behavior of multicopters. Arduino and Python code was developed to enable individual propeller control using a similar method as an actual flight controller, allowing a wide range of testing scenarios. Each propeller can be held at a constant RPM for replicating basic maneuvers such as hover, yaw, bank, and pitch. Transient analysis is also capable utilizing RPM sweeps and entire flight emulation. A flight log from a multicopter can be uploaded to replicate the behavior of a multicopter in an outdoor environment.

4. MEASUREMENT SETUP

All measurements were conducted in the hemi-anechoic chamber located at the University of Kentucky. The chamber dimensions are 6.1 m × 6.1 m × 3.0 m and meets the ISO requirements for

acoustic testing at 150 Hz and above. Two measurement systems were used for testing in the near and far fields.

4.1. Sound Pressure

Siemens LMS Testlab software and a Siemens SCADAS 8 channel data acquisition (DAQ) were used with PCB pressure microphones to measure the acoustic response. Half-inch microphones were placed at 0, 45, 90, and 270 degrees as detailed in Figure 4. All microphones were placed in the same horizontal plane located at the center of the propellers, approximately 1.1 m off the floor. Each microphone was placed 2 meters away from the propeller surface, a distance over 10 times the radius of the propellers.

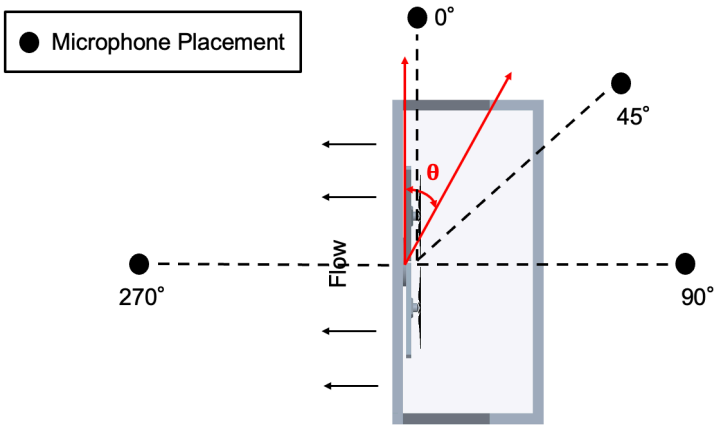

Figure 4. Far field measurement setup.

4.2. Scan & Paint 3D

The Microflown Scan&Paint 3D solution is a portable measurement tool capable of visualizing an acoustic field in three-dimensions [9]. The equipment can be seen in Figure 5 and is described below.

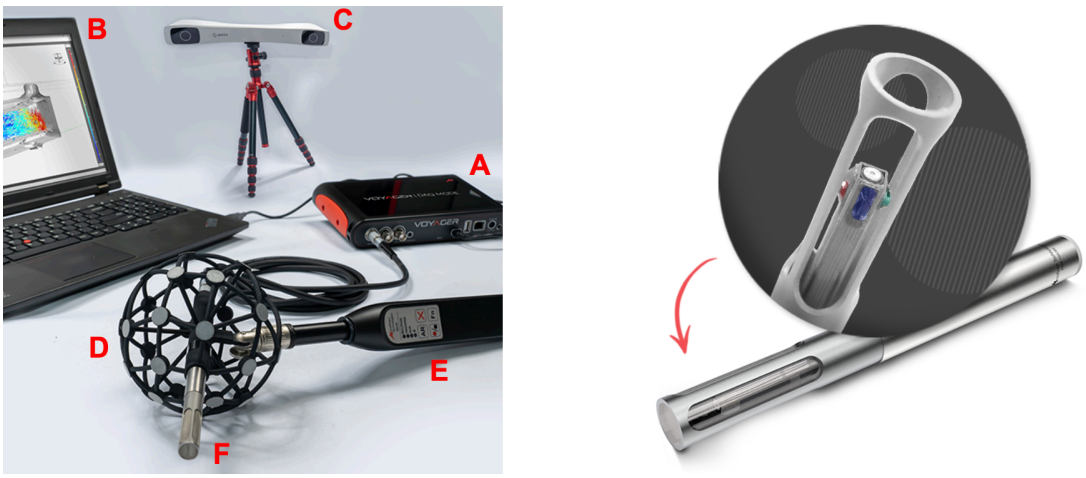

Figure 5: Microflown Scan&Paint 3D solution (left) and 3D sound intensity probe (right).

A. Microflown Voyager - A portable NVH analyzer and data acquisition system (DAQ).
B. Laptop with Scan&Paint 3D software (Velo)
C. PST Iris optical tracking camera
D. Tracking sphere containing randomly spaced reflectors.
E. Remote for single user measurement control
F. Microflown ½ inch 3D sound intensity probe (Frequency range 20 Hz – 10 kHz).

The 3D sound intensity probe is manually roved along the measurement surface as the recorded signals and position in space is synchronized in real-time. The sound field is then discretized into a cuboid grid over a 3D model of the object under test. The direction (sound intensity and particle velocity vectors) and magnitude of the sound field can then be calculated using the discretized sound pressure and orthogonal particle velocity signals [10].

5. RESULTS

Sound pressure in the far field was examined to compare the acoustic behavior of the test stand to known and established results. The impact from the test stand frame and a measurement safety grid was then determined with sound intensity scans in the near field.

5.1. Initial Measurements

Initial measurements were completed to ensure the test stand was effectively replicating the acoustic behavior of a quadcopter. The acoustic response of the propellers rotating at three different RPMs and the background noise in the anechoic chamber is plotted in Figure 6. This case is from the microphone located at 90°, perpendicular to the propeller plane on the top side of the propeller. Tonal propeller noise is the primary acoustic component for each of the three cases. Increases in the tonal peak-to-peak magnitude are observed as the rotational speed is increased, resulting in higher overall sound pressure levels for each increase in RPM. The propeller noise masks other sources, with the exception for the 1,960 RPM case, when noise from the test stand is visualized at approximately 2 kHz.

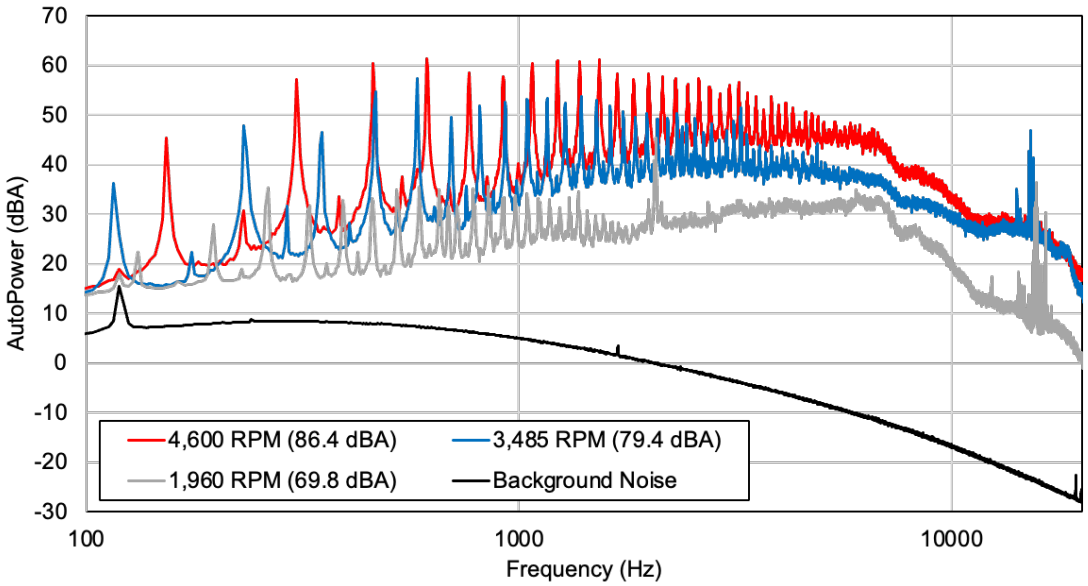

Figure 6: Acoustic response and OASPL of the UAV test stand operating at three different RPMs.

When operating a propeller/s in an enclosed space the unsteady flow initially generated by the propeller downwash is reintroduced into the propeller path. This flow recirculation can significantly increase the BPF harmonics and broadband noise, skewing the measurement data. Hence, static propeller testing is prone to elevated noise due to blade-turbulence interactions. Unlike in actual flight conditions, the propellers intersect each turbulent eddy for many revolutions at the same region of the blade surface, producing increased periodic surface pressure fluctuations [11]. This is likely the cause of the elevated harmonics of the BPF seen in Figure 6.

The directionality of the top, suction side, of the test stand is plotted in Figure 7. The microphone at 0 degrees is shown in gray, 45-degrees in red, and 90-degrees in blue. The lowest

acoustic response occurs in the propeller plane. Note that the OASPL from the 45-degree microphone is over 5 dB higher than the 90-degree. This increase in magnitude appears to be the result of broadband noise, possibly due to an increase in unsteady random loading noise along the 45-degee plane [11].

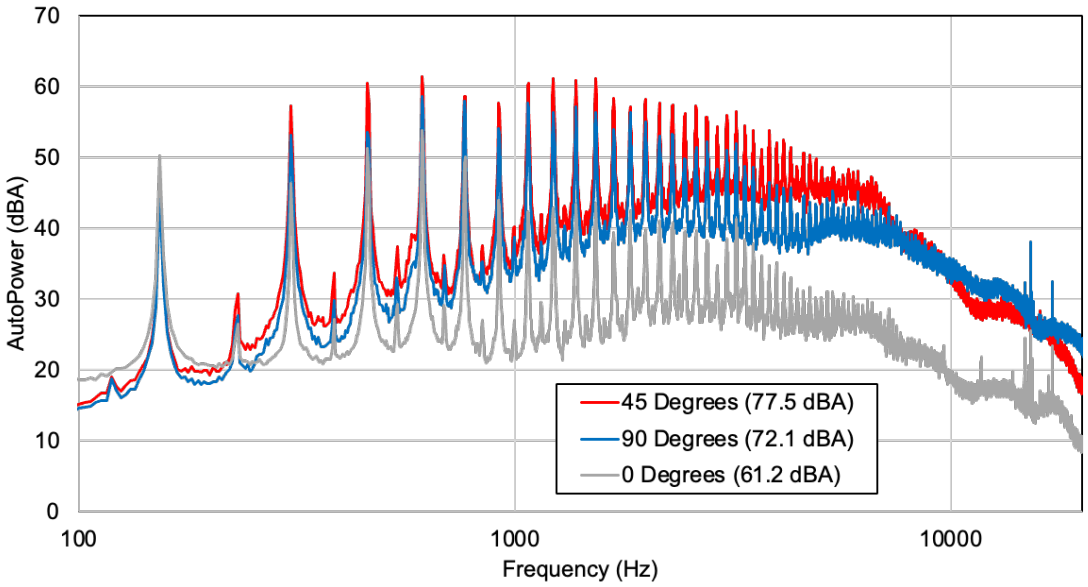

Figure 7: Directivity of the top side of the UAV test stand.

Figure 8 compares the top, suction side, of the test stand to the bottom, flow side. As previously discovered, the overall sound pressure level is greatest on the top of the quadcopter [12]. The high flow rate on the bottom of the propellers causes broadband flow-induced noise in the measurement, partially masking the tonal response, up to 1000 Hz.

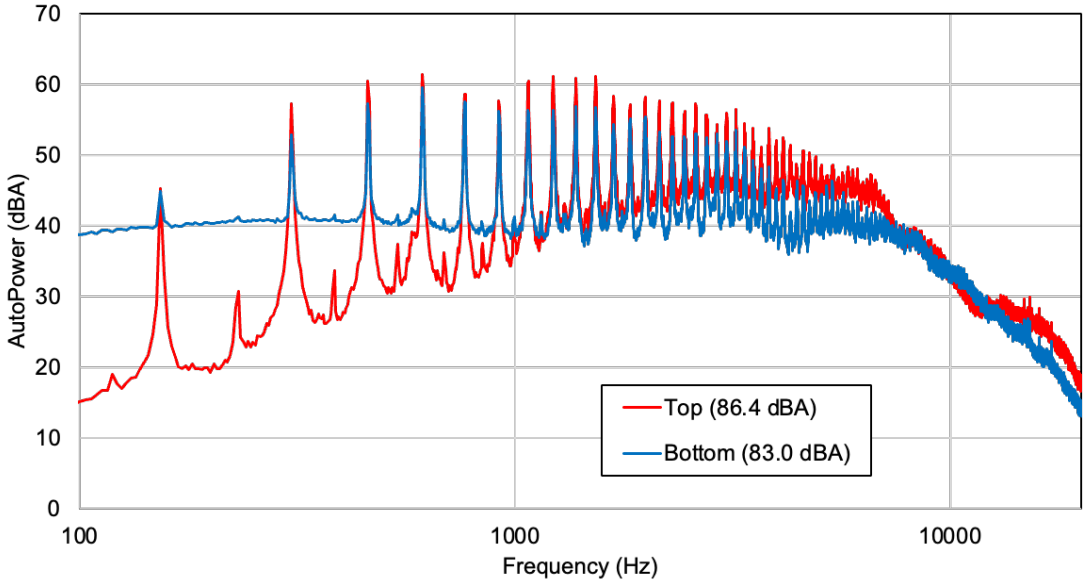

Figure 8: Acoustic response of the top and bottom of the UAV stand.

Maneuvers can be simulated by adjusting the RPM of motor pairs [13]. Figure 9 characterizes a constant bank maneuver, not including the transient response from hover to bank. The red curve is a standard hover while the blue curve is a simulated bank maneuver, resulting in two separate blade pass frequencies at each RPM of the motor pairs. The overall sound pressure level remains very

similar for both cases, but the tonal magnitude is decreased. Similar results were discovered when simulating yaw and pitch maneuvers.

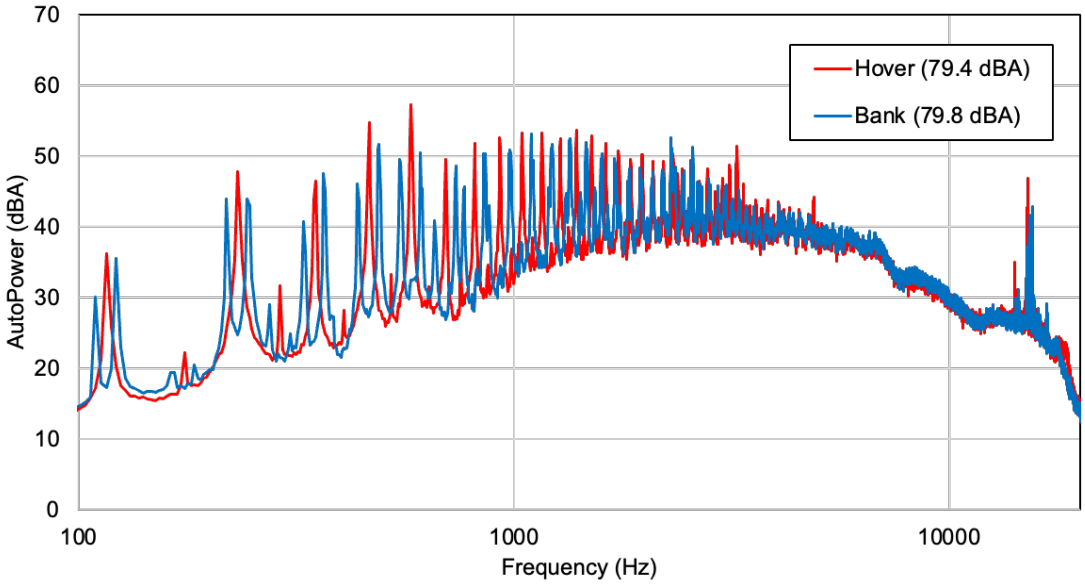

Figure 9: Simulated bank maneuver using the UAV test stand.

5.2. Frame Contribution

Scan&Paint 3D was used to measure the UAV stand arms while all four BLDC motors were operating at approximately 8300 RPM without blades. This was done to excite the stand and determine the acoustic response of the frame. The active and reactive sound intensity is visualized in Figure 10 at the sixth harmonic of the shaft rotational frequency. The sixth harmonic has a high amplitude due to a vented motor casing containing six support beams. The active sound intensity vectors in the near field follow the rotational direction of each motor, while the reactive sound intensity propagates normal from each source.

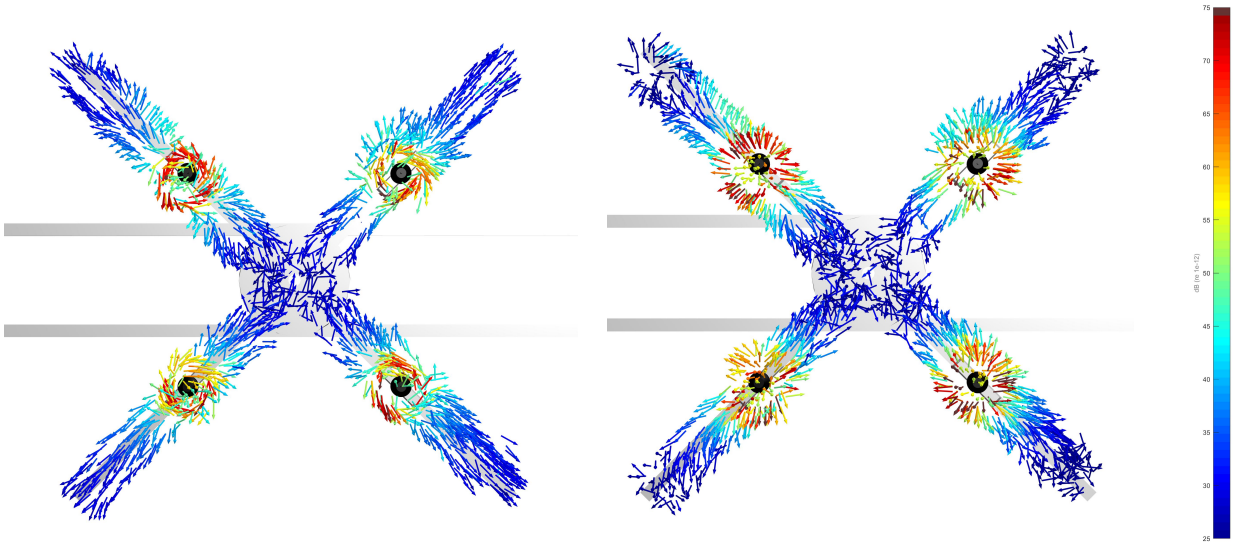

Figure 10: Active (left) and reactive (right) 3D sound intensity visualization.

The spatially-averaged sound intensity power spectrum is shown in Figure 11. The spectrum from the entire measurement is shown in red and isolated results from the test stand arms are shown in black. The acoustic contribution of the test stand is clearly indicated, which dominates the sound

field created by structural resonances at 1945 Hz, 3891 Hz, and 5859 Hz. The airborne motor noise masks the structure-borne frame radiation for the majority of the remaining frequencies.

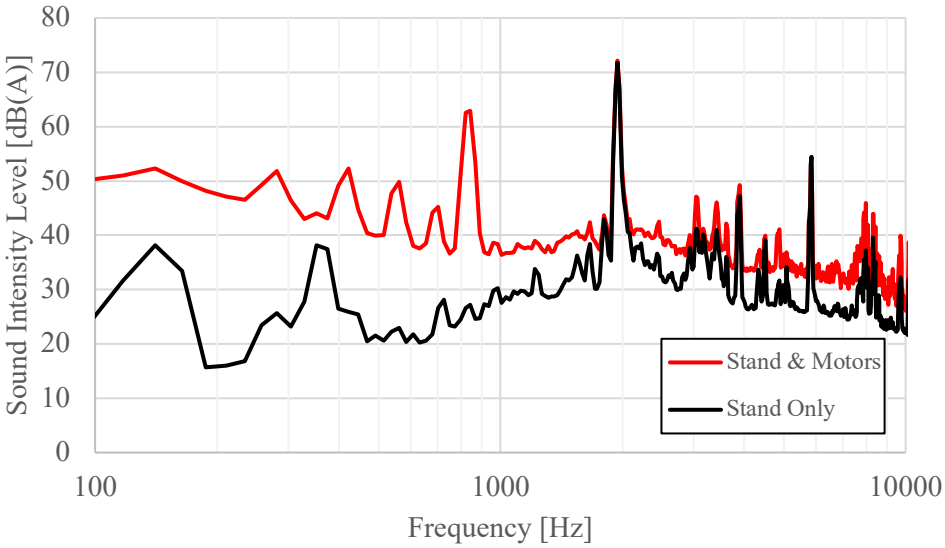

Figure 11: Power spectrum of the test stand and the isolated response from the test stand arms.

The active sound intensity at the two most significant test stand resonances, 1945 Hz (left) and 5859 Hz (right), is shown in Figure 12. It is observed that the motors are not the primary source as sound radiates along the length of the arms at these frequencies.

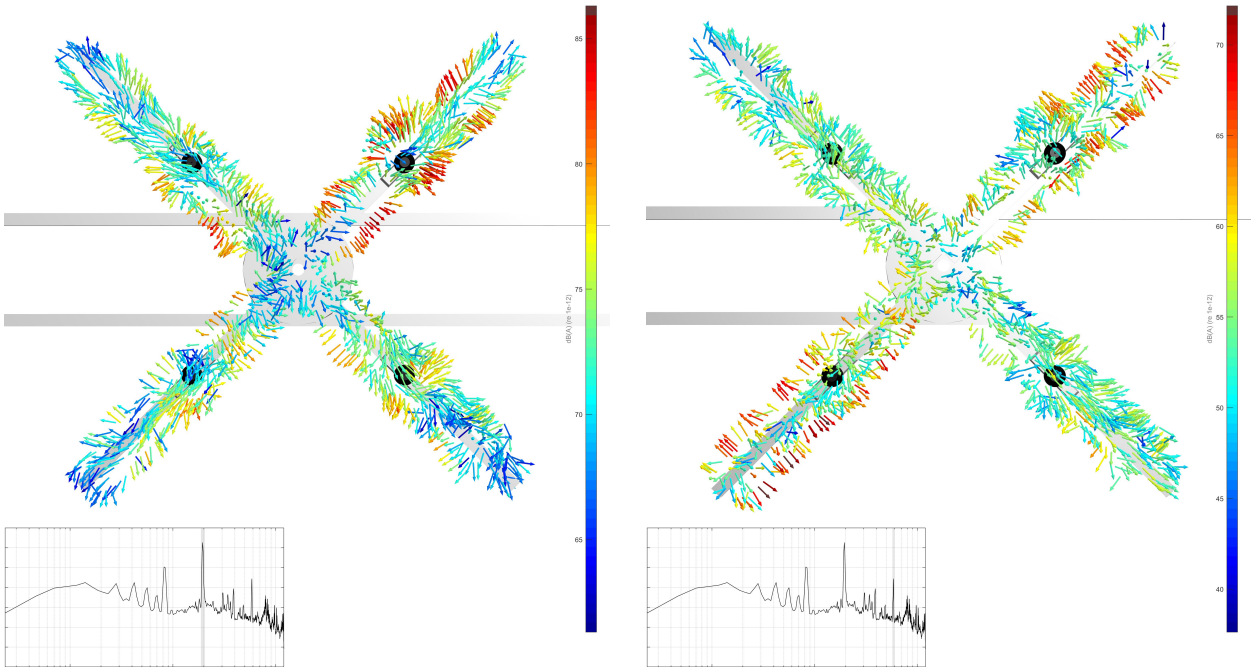

Figure 12: Active sound intensity direction and amplitude visualization at the test stand resonances: 1945 Hz (left) and 5859 Hz (right).

5.3. Grid Contribution

A safety grid was constructed for sound intensity scans on the test stand. The frame prevents potential impacts with the propellers when measuring in the near field as well as provides a scanning grid for uniform data collection. The frame can be seen in Figure 13 and is constructed from 1.9 cm × 3.8 cm wood slates with nylon string grids spaced 7.5 cm apart.

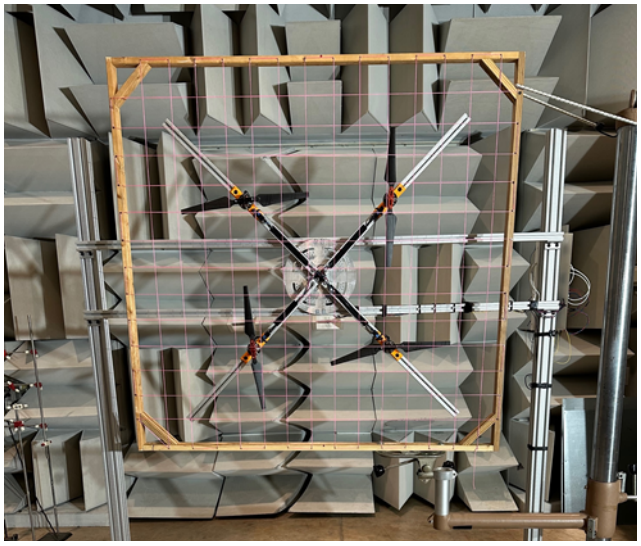

Figure 13: Safety grid used for sound intensity scans.

The safety grid was analyzed to understand the acoustic impact on the overall results. For the case when the test stand is used to measure acoustic propagation, the edge of the safety grid is effectively acting as another motor arm on the top, suction side of the propeller. Scan & Paint 3D was used to measure the propagation plane perpendicular to the propeller as the distance between the safety grid and the propeller surface was increased. This distance was measured using Equation 2, a unitless ratio of the tip clearance (the distance between the grid edge to the propeller surface) divided by the radius of the propeller. The broadband particle velocity when the grid edge is approximately 2.5 and 11.5 cm from the propeller surface, corresponding to a ratio of 0.13 and 0.6, is plotted in Figure 14. An increase in tonal noise starting from the second harmonic of the BPF is due to the blade passing over the static edge of the safety grid twice per revolution.

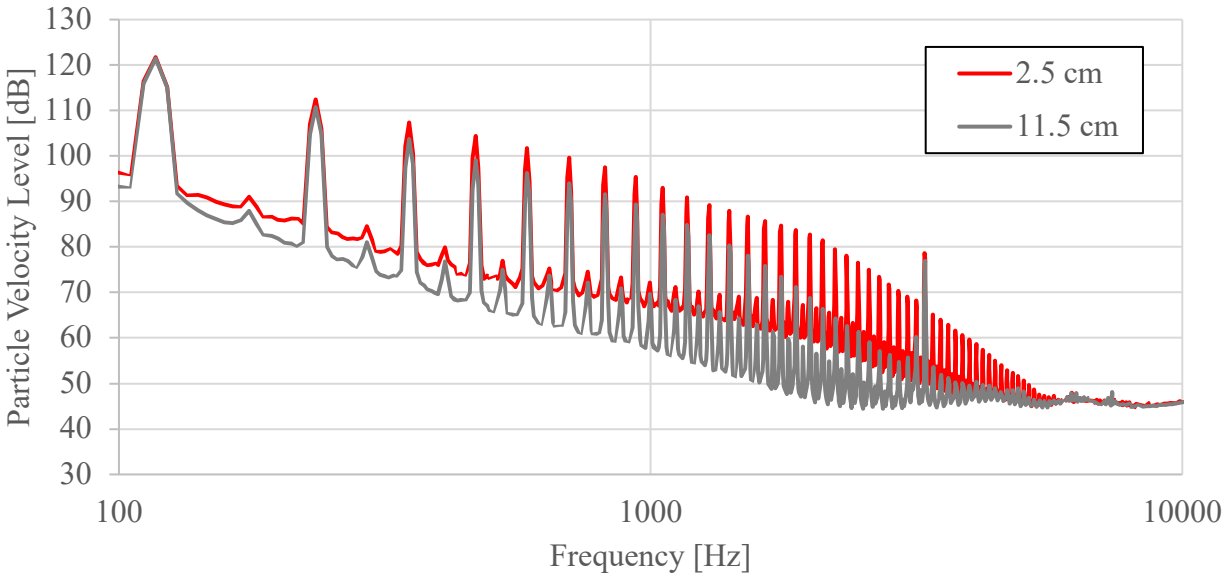

Figure 14: Particle velocity when the distance between the safety grid edge and propeller surface is 2.5 and 11.5 cm.

The overall particle velocity level of each measured distance is shown in Figure 15. Significant increases in overall levels occur when the safety grid is placed close to the propeller surface. Maintaining a ratio equal to or greater than 0.4 results in minimal influence from the safety grid.

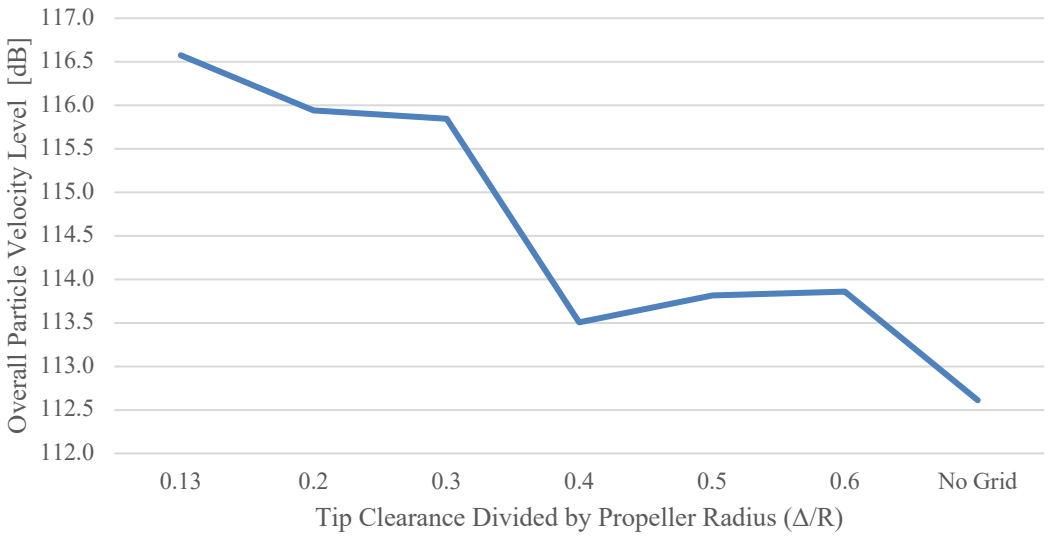

Figure 15: Overall particle velocity levels as the distance of the safety grid edge to the propeller surface is increased.

6. CONCLUSIONS

A UAV test stand was designed and constructed to enable safe and efficient testing in the near and far field. The test stand was developed to closely replicate the acoustics of a multicopter while maintaining flexibility for future measurement campaigns. A variety of multicopter configurations and hardware can be rapidly interchanged to obtain additional experimental data. The impact from the testing environment, the influence of the test stand, and a safety grid was analyzed. While measurements are likely skewed due to static propeller testing effects, interaction noise, and the test stand self-noise, the results provide valuable information. Measurement data using the UAV test stand, especially sound intensity scans in the near field, revealed interesting phenomena which will aid in further understanding the acoustic behavior of multicopters.

ACKNOWLEDGEMENTS

The authors gratefully acknowledge the support from the Vibro-Acoustics Consortium and Microflown Technologies.

REFERENCES

[1] Q. Quan, *Introduction to Multicopter Design and Control*. Singapore: Springer, 2017.

[2] N. Intaratep, W. N. Alexander, W. J. Devenport, S. M. Grace, and A. Dropkin, “Experimental Study of Quadcopter Acoustics and Performance at Static Thrust Conditions,” in *the 22nd AIAA/CEAS Aeroacoustics Conference*, Lyon, France: American Institute of Aeronautics and Astronautics, 2016.

[3] M. J. Crocker and J. P. Arenas, *Engineering Acoustics - Noise and Vibration Control*. Wiley, 2021.

[4] M. Šustek and Z. Úředníček, “The Basics of Quadcopter Anatomy,” *MATEC Web Conf.*, vol. 210, p. 01001, 2018.

[5] T. A. Brungart, S. T. Olson, B. L. Kline, and Z. W. Yoas, “The Reduction of Quadcopter Propeller Noise,” *Noise Control Engineering Journal*, vol. 67, no. 4, pp. 252–269, 2019.

[6] Y. Wu, M. J. Kingan, and S. T. Go, “Propeller–Strut Interaction Tone Noise,” *Physics of Fluids*, vol. 34, no. 5, p. 055116, 2022.

[7] N. S. Zawodny and D. D. Boyd, “Investigation of Rotor–Airframe Interaction Noise Associated with Small-Scale Rotary-Wing Unmanned Aircraft Systems,” *Journal of the American Helicopter Society*, vol. 65, no. 1, pp. 1–17, 2020.

[8] S. Watkins, N. Kloet, and X. Wang, “A Study of the Influence of Support Structure on Drone Noise,” in *QUIET DRONES International e-Symposium on UAV/UAS Noise*, 2020.

[9] “Scan&Paint 3D | Visualizing 3D Sound Intensity,” *Microflown Technologies*. https://www.microflown.com/products/sound-localization-systems/scan-paint-3d

[10] D. F. Comesanã, S. Steltenpool, M. Korbasiewicz, and E. Tijs, “Direct Acoustic Vector Field Mapping: New Scanning Tools for Measuring 3D Sound Intensity in 3D Space,” presented at the EuroNoise, 2015.

[11] M. J. Crocker, Ed., *Handbook of Noise and Vibration Control*. Hoboken, N.J: John Wiley, 2007.

[12] G. Cheng, J. Li, and D. W. Herrin, “UAS Sound Level Prediction using Panel Contribution Analysis,” in *QUIET DRONES International e-Symposium on UAV/UAS Noise*, 2020.

[13] R. Niemiec and F. Gandhi, “Multirotor Controls, Trim, and Autonomous Flight Dynamics of Plus- and Cross-Quadcopters,” *Journal of Aircraft*, vol. 54, no. 5, pp. 1910–1920, 2017.